Constructing Anode Ca-rich Protective Layer of for High Performance Aqueous Zinc-ion Batteries

Lun Zhang[a], #, Zhuo Chen[b], #, Junrun Feng[b], Hao Gu[a], Lin Sheng[c], Zhangxiang Hao[a], Feng Ryan Wang*, [a]

[a] Materials and Catalysis Laboratory, Department of Chemical Engineering, University College London, London WC1E 7JE, United Kingdom
[b] School of Science, School of Chip Industry, Hubei University of Technology, Wuhan, Hubei 430068, China
[c] School of Mechanical and Electronic Engineering, Suzhou University, Suzhou, Anhui 234000, China

Experimental

Materials preparation

Electrolyte preparation

The electrolytes used in the experiments were all 2 M $ZnSO_4$ solutions and 3.2294 g of zinc sulphate ($ZnSO_4$ Macklin 92 %) was added to 10 ml of deionized water to obtain the $ZnSO_4$ electrolyte.

Anode preparation

The zinc anodes in the experiment were divided into blank and experimental groups. Blank group: The bare Zn used in the experiment were all circles with a diameter of 12 mm. The cut bare Zn (100 μm) were ultrasonically cleaned with anhydrous ethanol (Macklin 99 %) for 15 min and then dried at 60 °C for 12 h to obtain the zinc anodes used in the experiment.

Experimental group: a solution of carboxymethyl cellulose (CMC) with a concentration of 10 mg mL^{-1} was prepared, and the resulting solution was mixed with $Ca_{10}(OH)_2(PO_4)_6$ (CHP) (Macklin) powder at a mass ratio of 9:1 to obtain a slurry, which was directly coated on processed zinc foils, with a thickness of 50 μm controlled by using a spatula, and dried for 2 h at 60 °C, to obtain a Zn@CHP anode.

Cathode preparation

The $NH_4V_4O_{10}$ powder synthesis method: One-step hydrothermal synthesis of $NH_4V_4O_{10}$ powder. More specifically, add 1.17 g of ammonium metavanadate (NH_4VO_3, Adamas, 99 %) to 70 ml of DI water and stir until thoroughly dissolved. Then 1.891 g of oxalic acid dihydrate ($H_2C_2O_4{\cdot}2H_2O$, SCRC, 99 %) was added into the solution and stirred at room temperature until the solution changed color. The mixed solution was transferred to Teflon-lined autoclave and heated at 140 °C for 720 h. After the reaction was completed, the $NH_4V_4O_{10}$ powder was washed with DI and dried at 70 °C for 12 h. $NH_4V_4O_{10}$ powder was firstly mixed with carbon black (C Aladdin 99.5%), polyvinylidene fluoride (PVDF) in a weight ratio of 7:2:1 and using 1-Methyl-2-pyrrolidinone (NMP Aladdin AR>99%) as solvent. The configured slurry was uniformly coated on the hydrophilic carbon cloth and dried at 60°C for 12 h before using, which was cut into discs with a diameter of 10 mm as cathodes. The loading of the $NH_4V_4O_{10}$ cathode was controlled to be about 2~3 mg cm^{-2}, and the additives were added to be 100 μL each time.

Battery assembly

All CR2032 coin cells were made with 19 mm diameter separators (Whatman GF/A), and cells with different electrodes and electrolytes were assembled at room temperature (25°C). Specifically, the Zn/Zn symmetric cell is an assembly of two zinc foils that serve as the cathode and anode, respectively. The full cell was $NH_4V_4O_{10}$ as the cathode (cathode preparation as described above), with a loading of 2~3 mg cm^{-2} per cathode, and the zinc foils served as anodes. Each time the cell was assembled 100 μL of electrolyte was added dropwise. The Coulombic efficiency of Zn/Cu half-cells with different electrodes was compared at a current density of 2 mA cm^{-2} area capacity of 1 mA cm^{-2} and a cut-off voltage of 0.5 V.

Materials characterization

The XRD patterns were obtained by Rigaku SmartLab 3KW X-ray diffractometer (Japan) and Cu Kα radiation in the 2θ range of 5° to 90° at 15° min^{-1}. The morphology and energy dispersive spectrometer (EDS) of the different zinc foil before and after electrochemical cycling was obtained by scanning electron microscope (SEM, SU8010). The *in-situ* optical microscope was conducted on RIEVBCAU MS4. The contact angles between different electrolytes and Zn electrodes were measured by using Dataphysics OCA 20 (German) with 5 μL of electrolyte for each test. XPS measurements of the Zn foil surface were conducted with a monochromatic Al Kα radiation (Thermo Fischer ESCALAB Xi+, American, 16 mA, 12.5 kV) under vacuum conditions. X-ray absorption near-edge structure (XANES) of Ca K edge (4.03keV) were carried out in BL20U, Shanghai Synchrotron Radiation Facility (SSRF, shanghai). Athena software was used for XANES analysis.

Electrochemical measurements

All electrochemical measurement dates were collected via the CHI660E and Corrtest electrochemical workstations. The Chronoamperometry (CA) was conducted with an overpotential of -150 mV within 300 s. Nucleation overpotential of Zn//Ti half-symmetric cell measured by linear sweep voltammetry (LSV) tested with a scan range from -0.4 to 1.3 V and a scan rate of 10 mV S^{-1}. The Tafel plots curve of the electrolyte was measured with a three-electrode system, with Zn foil as the working electrode, Pt foil as the counter electrode, and Ag/AgCl as the reference electrode. The test range was -1.3 to -0.7 V with a scan rate of 1 mV S^{-1}. Linear sweep voltammetry (LSV) investigations were carried out using a three-electrode system (WE: Zn@CHP or bare Zn; RE: Ag/AgCl; CE: Zn foil) in a 1.0 M Na_2SO_4 solution with 5 mV S^{-1} scan rate. The CV curves of $NH_4V_4O_{10}$/Zn full cells were measured with a scan range of 0.2-1.6

V and a scan rate of 1 mV S^{-1}. Electrochemical impedance spectroscopy (EIS) of all samples was measured using CR2032 coin cells within a frequency range between 0.01 Hz and 100000 Hz at a constant temperature.

Supporting Information Figures

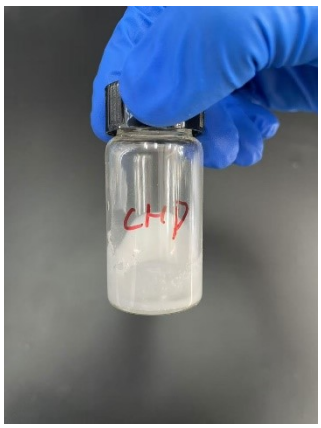

Figure S1. Image of slurry mixed with CMC and $Ca_{10}(OH)_2(PO_4)_6$ powder.

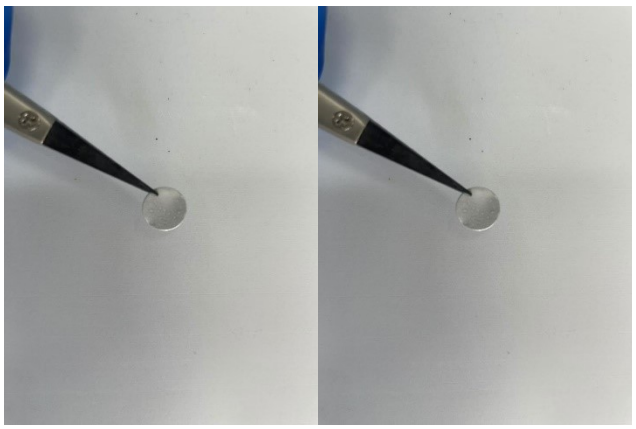

Figure S2. CHP coated zinc foil and bare Zn foil.

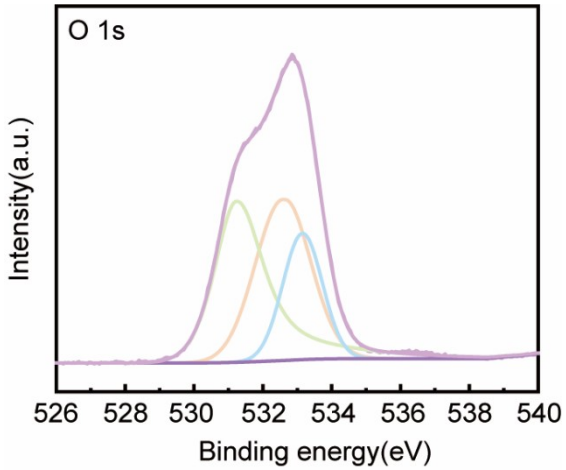

Figure S3. O 1s XPS spectrum for the surface of Zn@CHP anode before cycling.

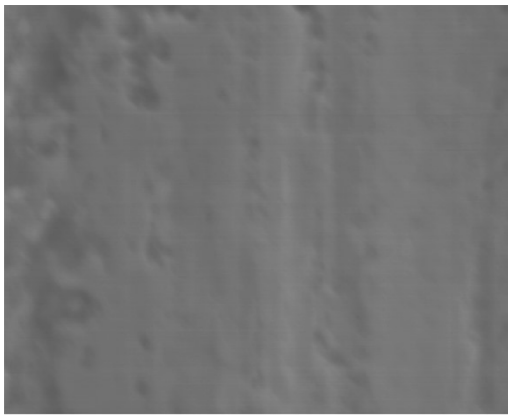

Figure S4. SEM image of Zn@CHP electrode surface after coating.

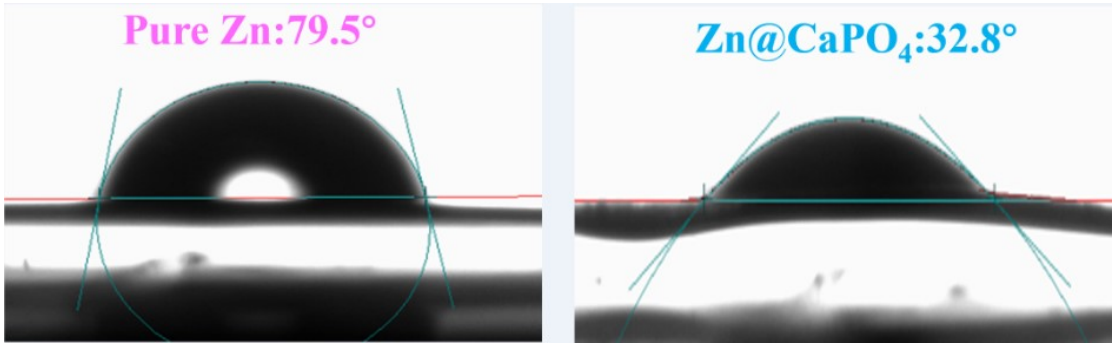

Figure S5. Contact angle of $ZnSO_4$ electrolyte on bare Zn and Zn@CHP.

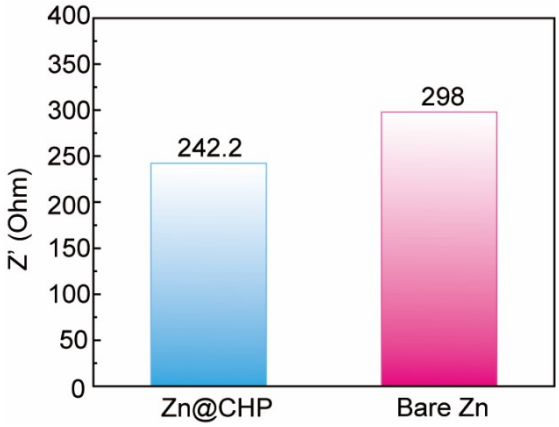

Figure S6 · EIS comparison of symmetric cells assembled with different electrode.

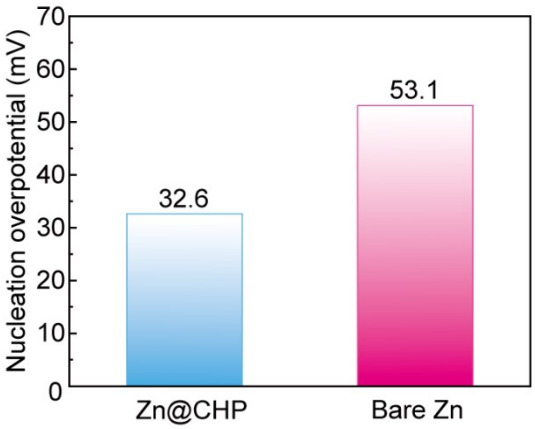

Figure S7. Comparison of nucleation overpotentials of Zn/Ti cells assembled with different electrode.

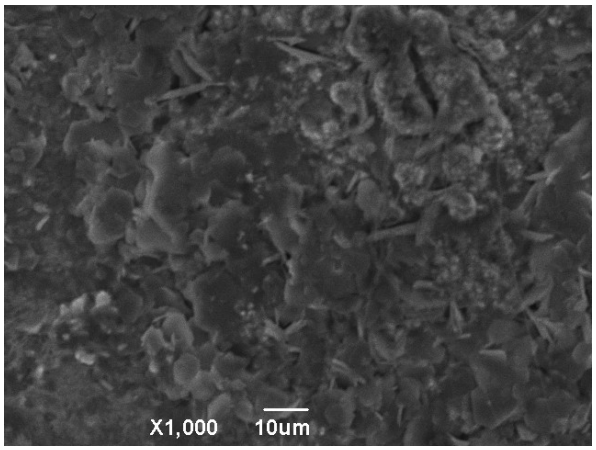

Figure S8. SEM images of bare zinc cycled 100 cycles at 15 mA cm^{-2} 2 mAh cm^{-2}.

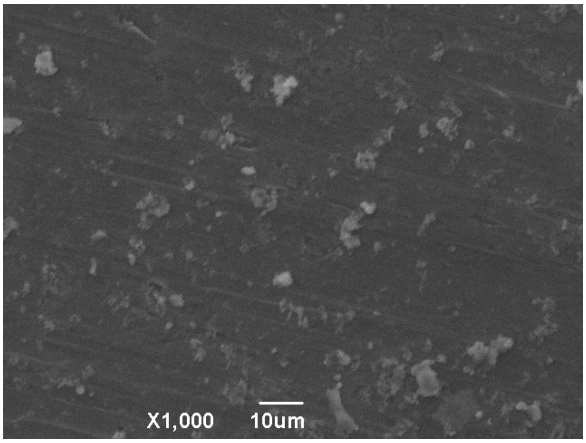

Figure S9. SEM image of Zn@CHP cycled 100 cycles at 15 mA cm^{-2} 2 mAh cm^{-2}.

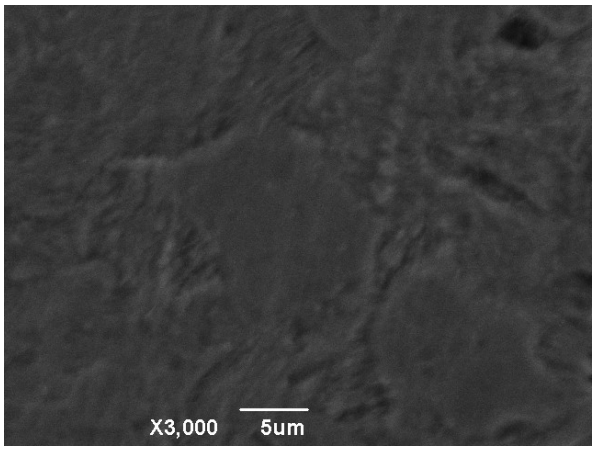

Figure S10. High-resolution SEM image of Zn@CHP cycled 100 cycles at 15 mA cm^{-2} 2 mAh cm^{-2}.

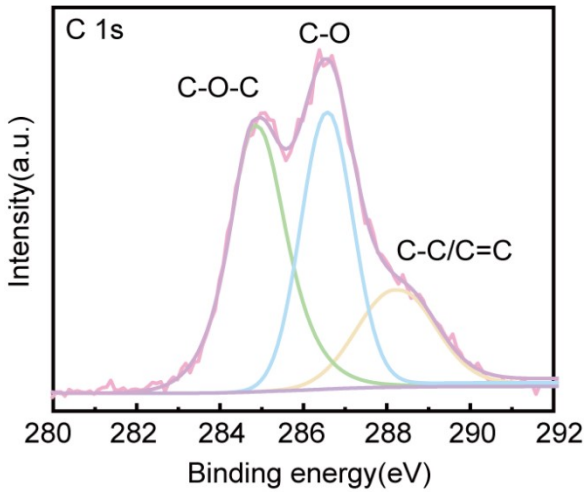

Figure S11. C 1s XPS spectrum for the surface of Zn@CHP anode after cycling.

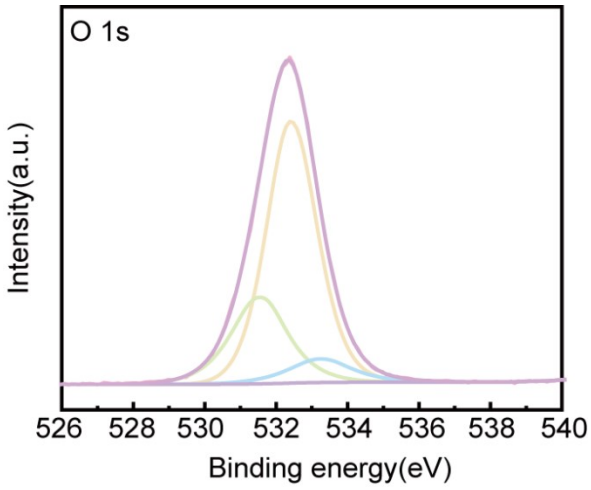

Figure S12. O 1s XPS spectrum for the surface of Zn@CHP anode after cycling.

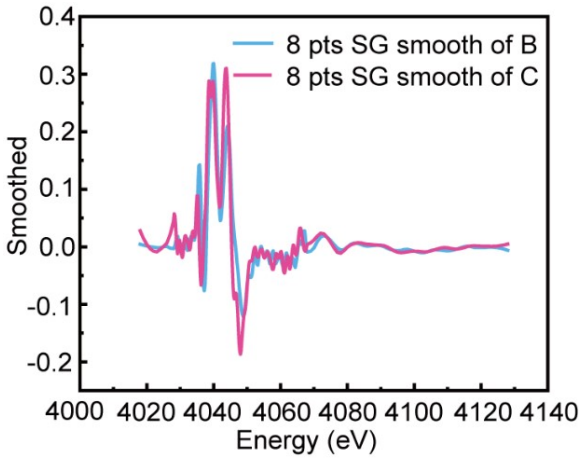

Figure S13. First derivative spectra of Zn@CHP before and after cycling.

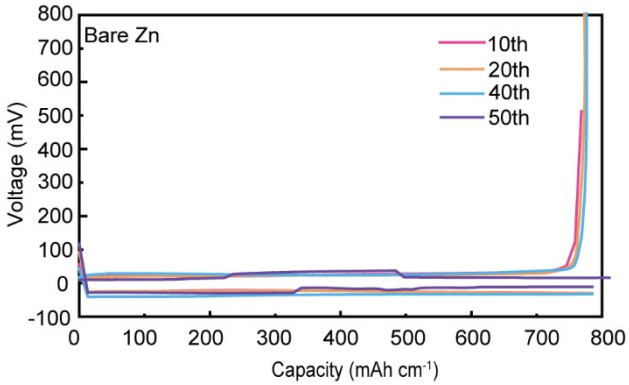

Figure S14. Voltage profiles at various cycles (10th, 20th, 40th, 60th) for the bare Zn anode.

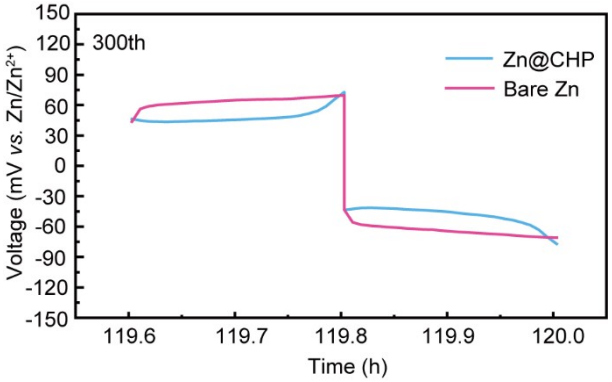

Figure S15. Comparison of overpotentials of different symmetric cells at 5 mA cm^{-2} at 300th cycles.

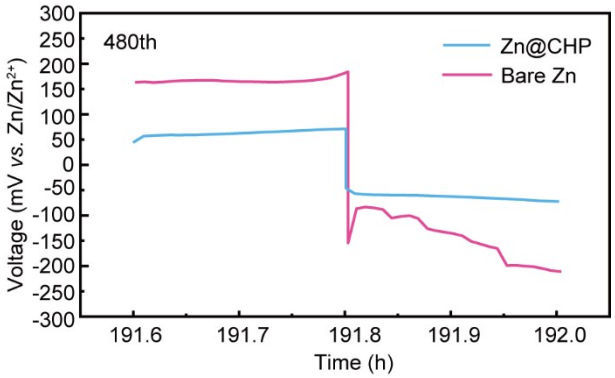

Figure S16. Comparison of overpotentials of different symmetric cells at 5 mA cm^{-2} at 480th cycles.

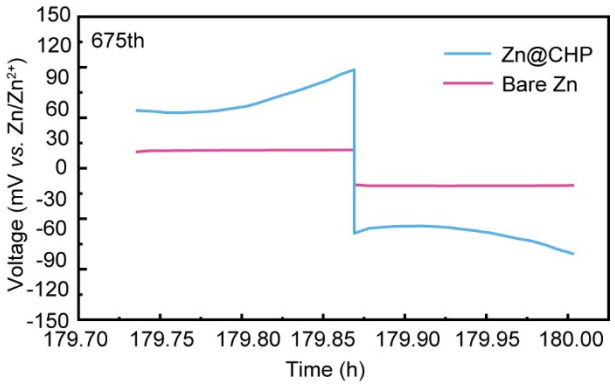

Figure S17. Comparison of overpotentials of different symmetric cells at 675th cycles at 15 mA cm^{-2}.

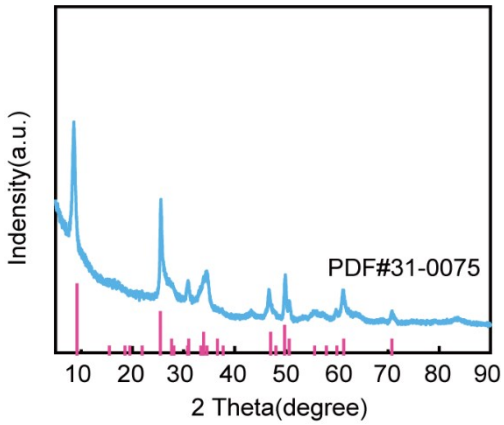

Figure S18. XRD pattern of synthesized NVO powder.

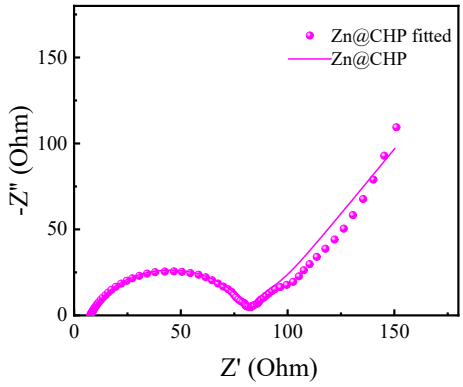

Figure S19. EIS test of full cell Zn@CHP/ $NH_4V_4O_{10}$.

Anode	Electrolyte	Mechanism	Performance	Ref.
ZnF_2-Cu@Zn		Effective inhibition of growth of severe dendrites by regulating Zn nucleation	1600 h at 0.5 mA cm^{-2} 0.5 mAh cm^{-2}	[1]
Bi-PVDF @Zn		3D cross-linking and dendrimer guides uniform Zn^{2+} deposition	2400 h at 1 mA cm^{-2} 1 mAh cm^{-2}	[2]
Zn@Sin		The Sn protective layer provides more robust Zn nucleation sites and higher HER potentials	500 h at 1 mA cm^{-2} 0.5 mAh cm^{-2}	[3]
Nb_2O_5@Zn		Nb_2O_5 guides Zn to be densely and uniformly oriented in a specific direction.	1000 h at 1 mA cm^{-2} 1 mAh cm^{-2}	[4]
Saturated fatty acid-zinc	$ZnSO_4$	Construction of zinc-friendly sites to dynamically regulate zinc nucleation and deposition behavior	2000 h at 1mA cm^{-2} 0.5 mAh cm^{-2}	[5]
Ti4O_7 @Zn		Prevents spontaneous corrosion of zinc anodes in the electrolyte, inhibiting HER and by-products.	2500 h at 1 mA cm^{-2} 1 mAh cm^{-2}	[6]
CA@Zn		The strong adsorption of anions on the Zn (002) plane prevents acid corrosion.	1600 h at 0.5 mA cm^{-2} 0.25 mAh cm^{-2}	[7]
Mxene@Zn		Mxene coating inhibits dendrite growth and undesired HER at the	————	[8]

	anode		
Ti@Zn	The coating contributes to the spatially uniform distribution of Zn nuclei and promotes dense Zn deposition	1100 h at 2 mA cm^{-2} 2 mAh^{-2}	[9]
Zn@CHP	regulate the homogeneous deposition of Zn^{2+}, reduce the nucleation potential of Zn,	1180 h at 5 mA cm^{-2} 1 mAh cm^{-2}	This work

Tables S1. Comparison of other published literature and this work.

Coating	Cycle life	Current density	CE	Ref
Nafion	>400 h	5 mA cm^{-2}	99.2%	[10]
$CaSiO_3$	>600 h	1.25 mA cm^{-2}	98.1%	[11]
Ni-Ag	>5000 h	1 mA cm^{-2}	99.77%	[12]
SnC_2O_4	>2300 h	1 mA cm^{-2}	99.56%	[13]
CHP	>1100 h	5 mA cm^{-2}	99.8%	This work

Table S2. Comparison with other published coating studies in terms of cycle life, current density, and CE.

References:

[1] Y. Mu, T. Zhou, D. Li, W. Liu, P. Jiang, L. Chen, H. Zhou, G. Ge, Highly stable and durable Zn-metal anode coated by bi-functional protective layer suppressing uncontrollable dendrites growth and corrosion, Chem. Eng. J. 430 (2022) 132839. https://doi.org/10.1016/j.cej.2021.132839.

[2] H. Lu, L. Liu, J. Zhang, J. Xu, Highly durable aqueous Zn ion batteries based on a Zn anode coated by three-dimensional cross-linked and branch-liked bismuth-PVDF layer, J. Colloid Interface Sci. 617 (2022) 422–429. https://doi.org/10.1016/j.jcis.2022.03.010.

[3] W. Guo, Y. Zhang, X. Tong, X. Wang, L. Zhang, X. Xia, J. Tu, Multifunctional tin layer enabled long-life and stable anode for aqueous zinc-ion batteries, Mater. Today Energy 20 (2021).

https://doi.org/10.1016/j.mtener.2021.100675.

[4] S. So, Y.N. Ahn, J. Ko, I.T. Kim, J. Hur, Uniform and oriented zinc deposition induced by artificial Nb2O5 Layer for highly reversible Zn anode in aqueous zinc ion batteries, Energy Storage Mater. 52 (2022) 40–51. https://doi.org/10.1016/j.ensm.2022.07.036.

[5] M. Fu, H. Yu, S. Huang, Q. Li, B. Qu, L. Zhou, G.C. Kuang, Y. Chen, L. Chen, Building Sustainable Saturated Fatty Acid-Zinc Interfacial Layer toward Ultra-Stable Zinc Metal Anodes, Nano Lett. 23 (2023) 3573–3581. https://doi.org/10.1021/acs.nanolett.3c00741.

[6] Y. Song, Y. Liu, S. Luo, Y. Yang, F. Chen, M. Wang, L. Guo, S. Chen, Z. Wei, Blocking the Dendrite-Growth of Zn Anode by Constructing Ti4O7 Interfacial Layer in Aqueous Zinc-Ion Batteries, Adv. Funct. Mater. 34 (2024) 1–10. https://doi.org/10.1002/adfm.202316070.

[7] L. Chen, F. Liu, Y. Dong, Y. Pei, X. Wang, X. Wu, X. Zheng, W. He, B. Long, Anion-induced facet-selective etching of Zn metal anode for long cycle aqueous Zn-ion batteries, J. Energy Storage 87 (2024) 111529. https://doi.org/10.1016/j.est.2024.111529.

[8] H. Luo, J. Jiang, Arramel, M. Li, K. Sun, Y. Zheng, Working mechanism of MXene as the anode protection layer of aqueous zinc-ion batteries, J. Colloid Interface Sci. 654 (2024) 289–299. https://doi.org/10.1016/j.jcis.2023.10.029.

[9] Y. Zhao, S. Guo, M. Chen, B. Lu, X. Zhang, S. Liang, J. Zhou, Tailoring grain boundary stability of zinc-titanium alloy for long-lasting aqueous zinc batteries, Nat. Commun. 14 (2023) 1–11. https://doi.org/10.1038/s41467-023-42919-7.

[10] L. Zhong, Y. Yan, Z. Ye, X. Zhang, W. Yang, J. Zheng, X. Lin, L. Zhang, G. Zhou, H. Lin, Z. Yuan, Covalent organic framework-mediated Nafion superhydrophobic coating for stabilizing the anode of aqueous zinc-ion batteries ☆, Chem. Eng. J. 527 (2026) 172018. https://doi.org/10.1016/j.cej.2025.172018.

[11] P. Zhai, X. Zhai, Z. Jia, W. Zhang, Inhibiting corrosion and side reactions of zinc metal anode by nano-CaSiO 3 coating towards high-performance aqueous zinc-ion batteries, Nanotechnology 34 (2023).

[12] Z. Yan, Q. Cheng, M. Sun, B. Wu, Bimetallic Modification Strategy : Ultra - Thin Ni - Ag Coating Prepared via One - Step Method Enables Highly Reversible Zn Anode, SmartMat (2025) 1–12. https://doi.org/10.1002/smm2.1323.

[13] A. Qiwei Gao, #, a Zhuo Chen, #, a Junrun Feng, *, a Xiaoyan Zhou, *, a Ziming Wan, a Lun Zhang, b Hao Gu, b Lin Sheng, c Pengfei Yao, a Feng Ryan Wang, b Zhangxiang Hao*, In-situ Generated Tin Protective Layers from

Stannous Oxalate for Dendrite-Free Zinc Anodes, Green Chem. (2025). https://doi.org/10.1039/D4GC06270A.